Application of the Adaptive Discontinuous Galerkin Method to Problems in Elastohydrodynamic Lubrication

H. Lu*, M. Berzins+ and P.K. Jimack*

*School of Computing, University of Leeds, UK
+School of Computing, University of Utah, USA

Abstract

Higher order discontinuous Galerkin methods offer the potential to solve both steady-state and transient problems efficiently and accurately. In this paper an introduction is provided to both elastohydrodynamic lubrication and the discontinuous Galerkin method before going on to describe the application of this method to the solution of typical problems, both steady-state and transient, that arise in elastohydrodynamic lubrication. In particular, it is demonstrated that the combination of high order elements and a simple spatial adaptive scheme can yield highly accurate numerical results using only hundreds of computational degrees of freedom.

Keywords: elastohydrodynamic lubrication, finite elements, discontinuous Galerkin, mesh adaptivity.

1   Introduction

Friction is an essential force that occurs in all aspects of our everyday life, allowing us to walk or making cars both run and stop for example. However, sometimes friction is not welcome: it can cause power loss in engines or reduce the lifetime of contacting elements (due to wear). In these situations, it is desirable that frictional forces should be minimised. The most common way to reduce friction and prevent wear is through lubrication, where lubricants are used to separate contacting surfaces, allowing the efficiency of components to be significantly enhanced and the lifetime of machine elements to be dramatically extended.

Since lubrication is such an effective way to reduce power loss and prevent wear, and since the behaviour of the lubricant film between contacting elements is of great importance in determining its performance, understanding this behaviour is of great interest to researchers. In many cases, the film thickness is determined exclusively by
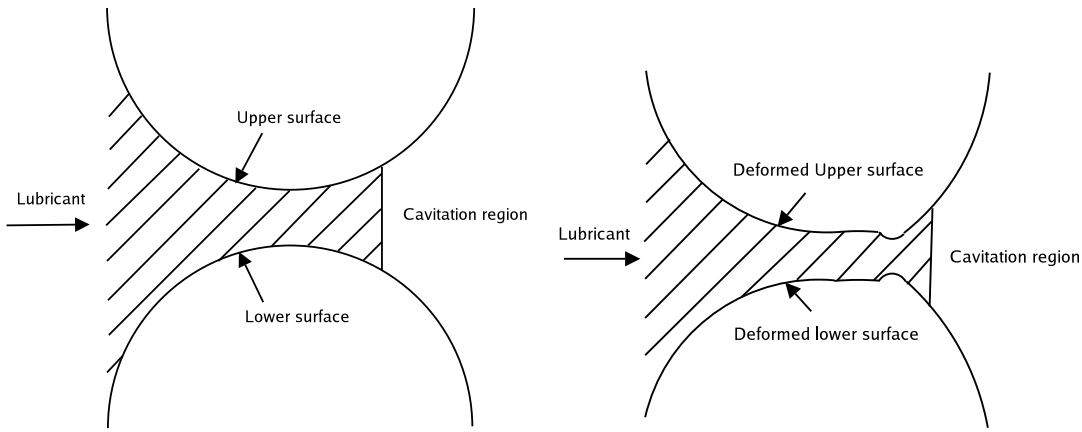
Figure 1: A schematic of hydrodynamic (left) and elastohydrodynamic (right) lubrication between two cylindrical surfaces.

the shapes of the contacting surfaces. This situation is called hydrodynamic lubrication, which is illustrated on the left of Figure 1 where the lubricant flows from left to right. However, when the pressure is sufficiently high, compared to the stiffness of the running surfaces, the elastic deformation of the contacting surfaces cannot be ignored, and this can heavily affect the shape of the lubricant film. The lubrication of such, more complicated, situations is referred to as *Elastohydrodynamic Lubrication* (EHL), which is shown on the right of Figure 1.

The EHL problem is not only characterised by the interaction between the film thickness and the elastic deformation. At such high pressures, the lubricant viscosity also depends heavily on pressure and the lubricant is compressible. A very interesting feature of the flow is a steep pressure spike that appears in the outlet region at high loads. The precise loading configuration affects both the shape and the position of the spike which can be very sharp indeed, although it is always smooth. Another important characteristic element of EHL is the outlet free boundary (or cavitation position) where the pressure of the lubricant becomes equal to the vapour pressure (conventionally taken to be zero). All of these features significantly increase the complexity of EHL problems compared to hydrodynamic lubrication problems. For a typical EHL contact problem, the desired information includes the pressure profile, the film thickness profile and the cavitation position.

In order to undertake theoretical analysis of EHL behaviour a common model problem that is considered is a contact between a paraboloid and a flat surface. According to the dimension of the contact, these problems are divided into two types: the line contact problem (1d) and the point contact problem (2d). Figure 2 shows the reduced geometry employed in the these two theoretical analyses, where: R, R_x and R_y are the radii of curvature; $h(x)$ and $h(x, y)$ are the film thickness, and; U_1 and U_2 are the velocities of the upper and the lower surfaces respectively. Throughout the rest of this paper we will only consider line contact problems for simplicity, however all of the techniques described can be extended naturally to point contacts.
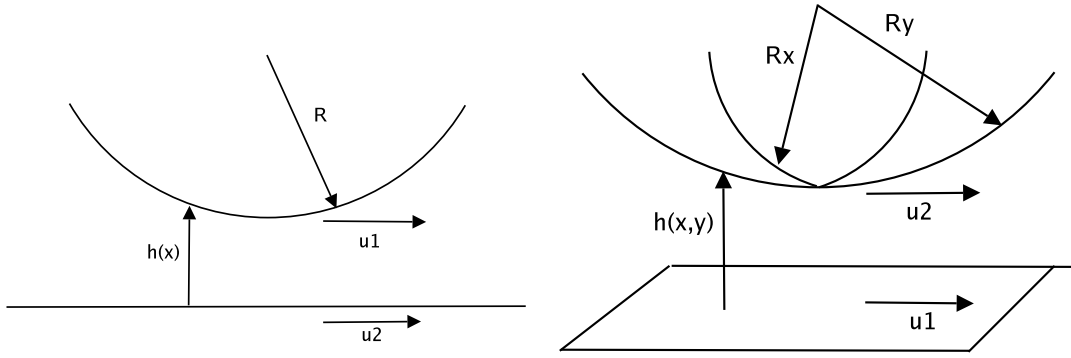
Figure 2: A schematic of line (left) and point (right) contacts.

In the following section further details are given concerning the nature of line contact problems, along with a brief description of their history and computational techniques that have been used to solve them numerically. Section 3 then introduces the discontinuous Galerkin method and illustrates how it may be applied to solve steady-state line contact EHL problems using mesh adaptivity. Section 4 then generalises these ideas to the solution of transient problems and the paper concludes with a short discussion of the work presented and how it may be further extended.

2 Background

2.1 Governing Equations

Due to the enormous variation in the magnitude of the key quantities within EHL models (up to $O(10^9)$ Pa for the pressure and down to $O(10^{-8})$ metres for the film thickness) it is necessary to consider non-dimensionalised systems of equations for the purposes of numerical simulation. In this section we define a typical non-dimensionalised model, further details of which may be found in [38] for example.

The first equation that we define is known as the Reynold's equation, which takes the following form:

$$\frac{\partial}{\partial X}\left(\epsilon\frac{\partial P}{\partial X}\right) - \frac{\partial(\rho H)}{\partial X} - \frac{\partial(\rho H)}{\partial T} = 0, \tag{1}$$

where

$$\epsilon = \frac{\bar{\rho} H^3}{\eta \lambda}, \tag{2}$$

$P(X)$ and $H(X)$ are the dimensionless pressure and film thickness respectively, $\rho(P)$ and $\eta(P)$ are the dimensionless density and viscosity, and λ is a dimensionless speed parameter.

3

The second equation is known as the film thickness equation, and this is given by:

$$H(X) = H_{00} + \frac{X^2}{2} - \frac{1}{\pi} \int_{-\infty}^{\infty} \ln|X - X'| P(X') \, dX', \tag{3}$$

where H_{00} is the dimensionless central offset film thickness and the integral describes the elastic deformation. Finally, a force balance equation is required:

$$\int_{-\infty}^{\infty} P(X) \, dX - \frac{\pi}{2} = 0. \tag{4}$$

The precise form used for the viscosity and density varies between models but for this paper we assume the following dimensionless forms (originally proposed in [34] and [8] respectively):

$$\eta(P) = e^{\{\frac{\alpha P_0}{z}[-1+(1+\frac{P P_h}{P_0})^z]\}} \quad \text{and} \quad \bar{\rho}(P) = \frac{0.59 \times 10^9 + 1.34 P P_h}{0.59 \times 10^9 + P P_h}. \tag{5}$$

Here, α, P_0, P_h and z are given constants: see [38], for example, for further details. Note that the form of equations (5) means that the value of ϵ in (2) can vary enormously, from very small to very large, in different parts of the computational domain. This means that in some regions equation (2) is convection-dominated and in others it is diffusion-dominated, which is a significant factor that must be accounted for by any numerical scheme that is applied.

For physical reasons, all pressures should be larger than or equal to the vapour pressure of the lubricant (taken to be zero for simplicity). This is not accounted for in the Reynolds equation, hence, in the outlet region, the calculated solution may have negative pressures. Consequently the Reynolds equation is only valid in the pressurised region and, the cavitation position, X_{outlet}, is therefore treated as a free boundary. Furthermore, in order to ensure that the model domain is finite the inlet boundary is fixed at a position X_{inlet}, that is sufficiently far from the contact region not to affect the nature of the flow. With this finite domain the associated boundary conditions are:

$$P(X_{inlet}) = 0, \quad P(X_{outlet}) = 0 \quad \text{and} \quad \frac{\partial P}{\partial X}(X_{outlet}) = 0. \tag{6}$$

2.2   Numerical Methods

The first numerical solution of the line contact problem, which simultaneously satisfied both the Reynolds equation and the film thickness equation, was obtained as long ago as 1951 by Petrusevich [32]. In this work a second maximum in the pressure profile was first observed, which now is referred to as "the Petrusevich spike" or "the pressure spike", and a corresponding dip in the film thickness was also obtained. These are regarded as the two major features of EHL solutions, which are not present when the contacting surfaces are presumed to be rigid. Figure 3 shows an illustration of a typical pressure spike.
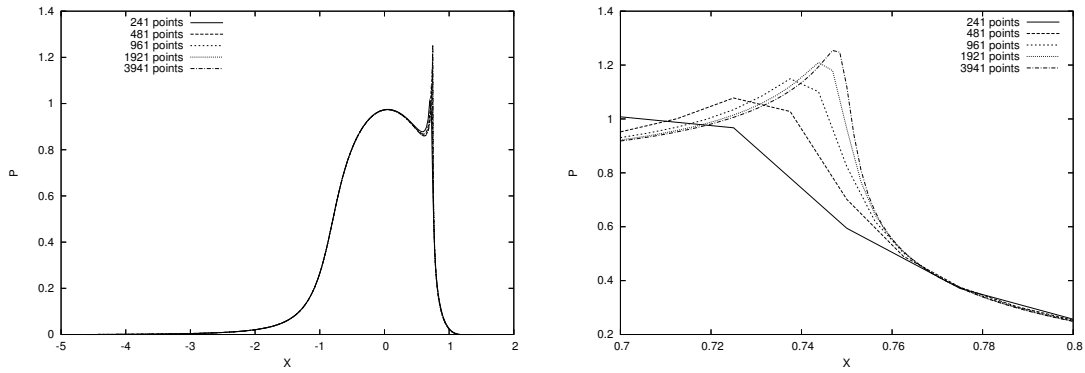
4

Figure 3: Typical finite difference results showing the full pressure profile (left) and details of the pressure spike (right).

Since the pioneering work of Petrusevich a wide variety of numerical methods have been applied to EHL problems. In 1959, Dowson and Higginson [7] introduced the inverse method which is mainly suitable for highly loaded cases. Evans and Snidle [13, 14] later extended this approach to point contact problems. Okamura applied the Newton-Raphson algorithm [30], and further improvements were made by Houpert and Hamrock [20] and Chang [6]. Another standard forward algorithm, Gauss-Seidel relaxation, was used by Hamrock and Dowson [16, 17] for both line contact and point contact problems. Unfortunately, both the Newton-Raphson and the Gauss-Seidel relaxation schemes are not particularly stable due to the extreme nonlinearity of EHL problems, particularly for highly loaded cases. To improve the stability, Evans [9] coupled the Reynolds equation and the film thickness equation together and solved for the pressure and the thickness simultaneously. To improve the efficiency, a so-called differential deflection method [12] was then introduced.

Over the past twenty years or so the most common approach that has been developed for the solution of EHL problems is based upon a combination of finite differences and multigrid. The multigrid method was first introduced for EHL problems by Lubrecht in 1986 [26] and, for the fast calculation of the elastic deformation Brandt and Lubrecht [2] developed a multilevel multi-integration (MLMI) algorithm which significantly reduces the computational complexity in approximating deformations at each point in the contact using (3). Figure 3 shows typical finite difference (FD) solutions computed on a range of grids. Finite element methods have only been used to a limited extent for the compressible EHL problems being considered here (although they have been applied more widely to the solution of incompressible EHL models, e.g. [37, 10, 29, 40, 27, 18, 19]). This is because some form of stabilisation is required in the compressible case (easily achieved via upwinding in FD schemes): for example, the solution is observed to oscillate in the contact region in [21] when a continuous quadratic finite element method (FEM) is used to discretise the Reynolds equation.

In the following sections we present a new FEM approach to EHL problems, based upon the discontinuous Galerkin method. This provides a means of combining the

5

advantages of high order approximation afforded by the FEM with the advantages of stability that have historically motivated the use of the FD method.

3 Discontinuous Galerkin for Steady-State Problems

3.1 Motivation

The original Discontinuous Galerkin (DG) method was introduced in 1973 by Reed and Hill [33] for solving a hyperbolic neutron transport equation. Indeed, most of the early work on DG methods was restricted to purely hyperbolic problems, for example [23, 31, 35, 3, 4, 5]. In 1998 a new DG method was introduced by Baumann and Oden [28, 1] that extended DG in a natural manner to second order convection-diffusion problems. Over each element boundary, both solution values and fluxes may be discontinuous. The continuity requirements over inter-element boundaries, and the boundary conditions, are imposed in a weak form. This treatment of inter-element boundaries prevents the appearance and spreading of numerical oscillations. For diffusion problems, this method was proved to be stable for polynomial basis functions of degree ≥ 3 and the L^2-rate of convergence found to be $O(h^{p+1})$ for p odd and $O(h^p)$ for p even. In convection-dominated cases, no artificial diffusion is required to improve the stability, which allows the order of accuracy to grow linearly with the order of the basis functions (assuming the underlying solution is smooth). So this is a high-order scheme which is applicable to both convection-dominated problems and diffusion-dominated problems. This property makes it an ideal candidate to be applied to equation (1) which can be both convection- and diffusion-dominated in different regions of the domain.

A further attraction of this DG method is the ease with which mesh adaptivity may be implemented. Since the solution is discontinuous over element interfaces, h-adaptivity can be easily performed without the restrictions imposed by the continuity requirements of the continuous FEM. Furthermore, the order of the approximating polynomial does not have to be the same for different elements. Hence, the implementation of p-adaptivity is very straightforward and natural. Of course, we can also adapt the grid concurrently with adjusting the polynomial degree of elements: this approach is generally referred to as h-p-adaptivity. In this particular paper only the use of h-adaptivity will be described.

3.2 Discretisation Details

The Reynolds Equation

When seeking steady-state EHL solutions the time-dependent term in the Reynolds equation (1) may be neglected, to leave

$$\frac{\partial}{\partial X}(\epsilon \frac{\partial P}{\partial X}) - \frac{\partial(\rho H)}{\partial X} = 0. \tag{7}$$

Let Ω_h be a partition of the domain $\Omega = [X_{inlet}, X_{outlet}]$ into N elements. Let $\Gamma_{int} = \cup \Gamma_{ef}$ denote internal interfaces between elements, where Γ_{ef} is the grid point separating elements e and f. We define the jump of a function v on the element interface Γ_{ef}

$$[v(x)]_{ef} = \lim_{x \to \Gamma_{ef}, x \in e} v(x) - \lim_{x \to \Gamma_{ef}, x \in f} v(x), \ e > f, \tag{8}$$

and the average

$$\langle v(x) \rangle_{ef} = \frac{1}{2} \left(\lim_{x \to \Gamma_{ef}, x \in e} v(x) + \lim_{x \to \Gamma_{ef}, x \in f} v(x) \right). \tag{9}$$

In each element e, P is approximated in the following form:

$$P^e(X) = \sum_{i=1}^{p^e+1} u_i^e N_i^e(X), \quad N_i^e(X) \in V \tag{10}$$

where p^e is the order of the approximating polynomial, u_i^e are the unknown coefficients and $N_i^e(X)$ are the local finite element basis functions which belong to a finite element space V. In this paper, a family of *hierarchical* basis functions are used, which was introduced in [36]. In the reference element the following basis functions are defined:

$$N_1(\xi) = \frac{1 - \xi}{2}; \quad N_2(\xi) = \frac{1 + \xi}{2}; \quad N_i(\xi) = \phi_{i-1}(\xi), \ i = 3, 4, \ldots, p+1 \tag{11}$$

where p is the polynomial degree of the elements and $\xi \in [-1, +1]$. Here ϕ_j is defined in terms of the *Legendre polynomial P_{j-1}*:

$$\phi_j(\xi) = \sqrt{\frac{2j-1}{2}} \int_{-1}^{\xi} P_{j-1}(t) \, dt, \quad j = 2, 3, \ldots \tag{12}$$

The basis functions N_1, N_2 are called *nodal shape functions or external modes*. The basis functions N_i ($i = 3, 4, \ldots, p+1$) are called internal shape functions or internal modes, sometimes: *bubble modes*. These basis functions are well suited for computer implementation of p-adaptivity because it is easy for us to enhance the accuracy of the solution by adding more hierarchical basis functions on some elements or to reduce the accuracy by dropping several highest order basis functions as appropriate. Some important properties of Legendre polynomials are listed in [36]. In particular, we have:

$$\phi_j(\xi) = \frac{1}{\sqrt{(2(2j-1))}} (P_j(\xi) - P_{j-2}(\xi)). \tag{13}$$

With the above formulae, it is easy to evaluate the internal basis functions. Figure 4 depicts the first 6 basis functions in the reference element.

Combining the above notation, the one-dimensional steady-state Reynolds equation (7) can be discretised into the following form:

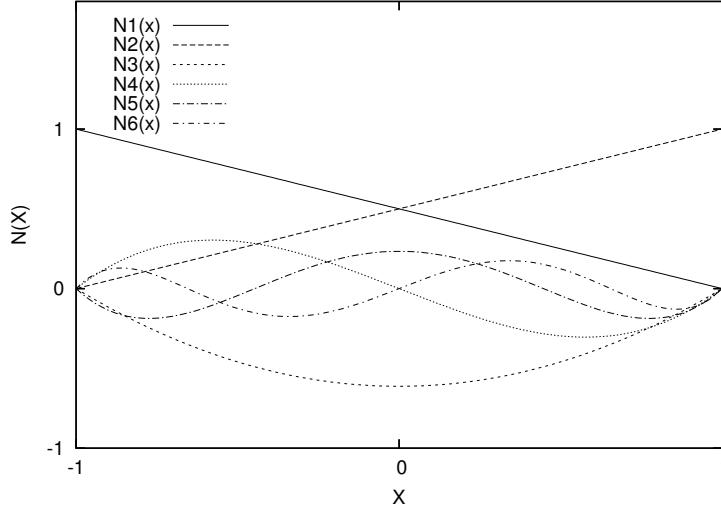$$L(P, v) = a(P, v) - l(P, v) = 0, \quad \forall v \in V, \tag{14}$$

Figure 4: One-dimensional basis functions on the reference element.

where

$$a(P, v) = \sum_{e \in \Omega_h} \left(\int_e \epsilon \frac{\partial P}{\partial X} \frac{\partial v}{\partial X} \, dX \right) + \sum_{\Gamma_{int}} \left([v] \langle \left(\epsilon \frac{\partial P}{\partial X} \right) \rangle - [P] \langle \left(\epsilon \frac{\partial v}{\partial X} \right) \rangle \right)$$
$$+ \left(v \epsilon \frac{\partial P}{\partial X} \right) |_{X_{inlet}} - \left(v \epsilon \frac{\partial P}{\partial X} \right) |_{X_{outlet}} - \left(P \epsilon \frac{\partial v}{\partial X} \right) |_{X_{inlet}} + \left(P \epsilon \frac{\partial v}{\partial X} \right) |_{X_{outlet}},$$

$$(15)$$

and

$$l(P, v) = \sum_{e \in \Omega_h} \left(\int_e \rho H \frac{\partial v}{\partial X} \, dx \right) + \sum_{\Gamma_{int}} [v] \langle \rho(P^-) H \rangle$$
$$+ (\rho H v) |_{X_{inlet}} - (\rho H v) |_{X_{outlet}} - \left(g_{inlet} \epsilon \frac{\partial v}{\partial X} \right) |_{X_{inlet}} + \left(g_{outlet} \epsilon \frac{\partial v}{\partial X} \right) |_{X_{outlet}}.$$

$$(16)$$

In the above equations,

$$P^- = \lim_{\sigma \to 0} P(x - \sigma), \quad \text{for } x \in \Gamma_{int}. \tag{17}$$

This provides sufficient upwinding to ensure a stable solution [1]. Note that in equation (15) $[v] \langle \epsilon \frac{\partial P}{\partial X} \rangle$ is nonzero after the integration by parts since v is discontinuous over each element boundary. The continuity condition of P over inter-element boundaries is implemented by requiring

$$\sum_{\Gamma_{int}} [P] \langle \left(\epsilon \frac{\partial v}{\partial X} \right) \rangle = 0, \tag{18}$$

8

see equation (15). Dirichlet boundary conditions are also imposed in a weak form:

$$(P - g_{inlet})\left\langle\left(\epsilon\frac{\partial v}{\partial X}\right)\right\rangle = 0 \quad \text{and} \quad (g_{outlet} - P)\left\langle\left(\epsilon\frac{\partial v}{\partial X}\right)\right\rangle = 0, \qquad (19)$$

see equation (16). (Note that for this problem, (6) implies that $g_{inlet} = g_{outlet} = 0$.)

The Film Thickness Equation

For a given pressure distribution the film thickness (3) may be calculated as follows:

$$
\begin{aligned}
H(X) &= H_{00} + \frac{X^2}{2} - \frac{1}{\pi}\int_{X_{inlet}}^{X_{outlet}} \ln|X - X'|P(X')\,\mathrm{d}X' \qquad (20)\\
&= H_{00} + \frac{X^2}{2} - \frac{1}{\pi}\sum_{e\in\Omega_h}\int_e \ln|X - X'|P(X')\,\mathrm{d}X'\\
&= H_{00} + \frac{X^2}{2} - \frac{1}{\pi}\sum_{e\in\Omega_h}\int_e \ln|X - X'|\sum_{i=1}^{p^e+1} u_i^e N_i^e(X')\,\mathrm{d}X'\\
&= H_{00} + \frac{X^2}{2} - \frac{1}{\pi}\sum_{e\in\Omega_h}\sum_{i=1}^{p^e+1}\int_e \ln|X - X'|N_i^e(X')\,\mathrm{d}X'\,u_i^e\\
&= H_{00} + \frac{X^2}{2} - \frac{1}{\pi}\sum_{e\in\Omega_h}\sum_{i=1}^{p^e+1} K_i^e(X)u_i^e,
\end{aligned}
$$

where the kernel values $K_i^e(X)$ are defined by:

$$K_i^e(X) = \int_e \ln|X - X'|N_i^e(X')\,\mathrm{d}X'. \qquad (21)$$

Here $K_i^e(X)$ may be calculated numerically. When X is outside of e, m-point Gaussian quadrature is used however when $X \in e$, singular quadrature must be employed (see, for example [11]) since $\ln|X - X'|$ has a weak singularity at $X' = X$.

In order to evaluate the integrals in equation (15) and (16), it is necessary to calculate the values of the film thickness at the quadrature points X_f^j, $j = 1, 2 \ldots, m$ (m is the number of the quadrature points in each element f) and at each element boundary X_k, $k = 1, 2, \ldots, N + 1$. Therefore, the kernels at the quadrature points, $K_i^e(X_f^j)$, and at the element boundaries, $K_i^e(X_k)$, are required. From (21), it can be seen that $K_i^e(X)$ depends only on the structure of the grid that is used and upon the basis functions. Hence, once the grid and the basis functions are fixed, $K_i^e(X_f^j)$ and $K_i^e(X_k)$ can be precomputed for maximum efficiency.

The Force Balance Equation

The force balance equation (4) is discretised according to:

$$\sum_{e \in \Omega_h} \int_e \sum_{i=1}^{p^e+1} u_i^e N_i^e(X) \, \mathrm{d}X - \frac{\pi}{2} = 0. \tag{22}$$

By introducing another kernel KK_i^e:

$$KK_i^e = \int_e N_i^e(X) \, \mathrm{d}X, \tag{23}$$

the discrete force balance equation can be rewritten as:

$$\sum_{e \in \Omega_h} \sum_{i=1}^{p^e+1} KK_i^e u_i^e - \frac{\pi}{2} = 0. \tag{24}$$

This kernel can also be precomputed, using Gaussian quadrature, for given a grid and basis functions.

3.3 Solution Method

Before discussing procedures for solving the discrete system of nonlinear algebraic equations derived above one further issue must be addressed. As already noted, the problem specified in subsection 2.1 is a free boundary problem, with the cavitation point X_{outlet} to be determined. One way of dealing with this free boundary is through the use of a penalty method, such as that applied in [40] for an incompressible EHL problem. By introducing an exterior penalty term, the following nonlinear system will be solved instead of (14):

$$L(P, v) = a(P, v) + \frac{1}{\delta} \sum_{e \in \Omega_h} \int_e P_- v \, \mathrm{d}X - l(P, v) = 0, \tag{25}$$

where δ is an arbitrary positive number and

$$P_- = min(P, 0). \tag{26}$$

Note that the penalty term $\frac{1}{\delta} \sum_{e \in \Omega_h} \int_e P_- v \, \mathrm{d}X$ is not effective where $P \geq 0$. In the outlet region however, the penalty term dominates the equation (25) when $P < 0$, provided that the δ is small enough. In this case, the negative pressures are forced to be zero by the penalty term in the weak form. Consequently, the condition $P \geq 0$ is satisfied over the entire computational domain and the cavitation position can be recovered from this solution if it is required.

Now, based upon (10) and (25) the discrete Reynolds equation may be written in the general form:

$$L(U) = A(U)U - b(U) = 0, \tag{27}$$

where

$$U = (u_1^1, \ldots, u_{p^1+1}^1; \ldots; u_1^N, \ldots, u_{p^N+1}^N) \tag{28}$$

are the unknown pressure coefficients. Note that both $A(U)$ and $b(U)$ depend on U. Since the entries of U are ordered element-by-element (see (28)), $A(U)$ is a block-tridiagonal matrix and the size of the each block is determined by the degree of the basis functions on the corresponding elements.

In order to solve this nonlinear algebraic system the following iteration is proposed:

$$U \leftarrow U + \left(\frac{\partial L}{\partial U}\right)^{-1} R, \tag{29}$$

where R is the numerical residual of the discrete Reynolds equation and $\frac{\partial L}{\partial U}$ is approximated by:

$$\frac{\partial L}{\partial U} = \frac{\partial A(U)U}{\partial U} - \frac{\partial b(U)}{\partial U} \tag{30}$$

$$\approx A(U) - \frac{\partial b(U)}{\partial U}. \tag{31}$$

Numerical experiments indicate that (31) provides a sufficiently robust smoother. Furthermore, the efficiency of this iteration may be improved significantly by approximating $\frac{\partial b(U)}{\partial U}$ in (31) by a block tridiagonal matrix which has the same sparsity pattern as $A(U)$. The justification for this comes from noting that in (16) the dependency on pressure is implicitly through the film thickness term H and that, by (20), H depends more strongly on the nearby pressures than those further away. Consequently, $\frac{\partial L}{\partial U}$ in (29) is approximated by a block tridiagonal matrix, which makes this matrix both cheap to compute and cheap to invert. In practise some under-relaxation may also be incorporated in (29):

$$U \leftarrow U + C_1 \left(\frac{\partial L}{\partial U}\right)^{-1} R. \tag{32}$$

Once a converged pressure solution is obtained for the discrete Reynolds equation, based upon an initial guess for H_{00} in (20), this unknown reference thickness must also be updated. This update is based upon the defect in the force balance equation (24):

$$H_{00} \leftarrow H_{00} - C_2(\frac{\pi}{2} - \sum_{e=1}^{N} \sum_{i=1}^{p^e+1} KK_i^e u_i^e), \tag{33}$$

where C_2 is an under-relaxation factor for H_{00}. With this new value of H_{00} the discrete Reynolds equation must be resolved and this iteration process repeated until H_{00} is converged.

A final ingredient that is required for an efficient solution scheme is the incorporation of mesh adaptivity. Here an automatic h-adaptive scheme is briefly described, allowing all of the features of EHL solutions to be captured with only a small number of elements. The underlying mechanism that is used to drive the adaptivity is based
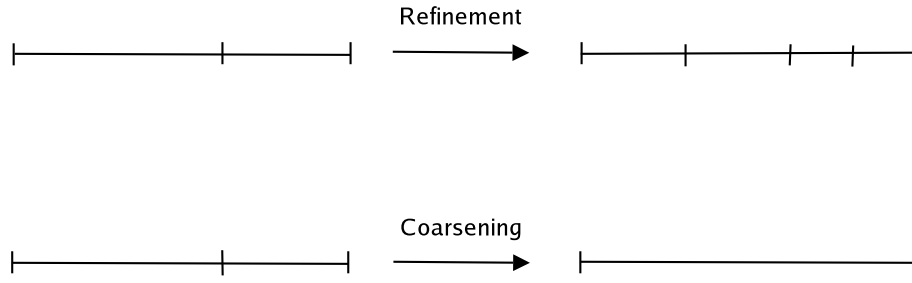
Figure 5: An illustration of refinement and coarsening.

upon an assumption that when the local mesh size is sufficiently small the components of the two highest degree basis functions, in the representation of the approximate solution, will be very small. The basic idea is as follows.

1. Suppose that the solution on an element e is such that $|u^e_{p^e+1}| < Tol_1$ and $|u^e_{p^e}| < Tol_1$ (see (10)), where Tol_1 is a given tolerance, then refine this element by splitting it into two equally spaced smaller elements. See the upper case in Fig 5 for an illustration of two elements being split in this manner.

2. Alternatively suppose that two neighbouring elements, e and f say, can be agglomorated to form one larger element, E. Then if the interpolated solution on this new element is such that $|u^E_{p^E+1}| < Tol_2$ and $|u^E_{p^E}| < Tol_2$, where $Tol_2 < Tol_1$ is also a given tolerance, then accept this coarsened element. See the lower case in Fig 5.

This simple h-adaptive algorithm has been incorporated into the solution procedure for the results that appear in the following subsection.

3.4 Computational Results

We conclude this section with a selection of typical numerical results that demonstrate the ability of the proposed DG method to capture all details of an EHL solution, even when the applied load is sufficiently large to cause a significant elastic deformation and a very sharp pressure spike. Similar results are also presented by the authors in [24], where comparison is made against finite difference solutions computed on very fine meshes in order to demonstrate the accuracy of the DG results obtained.

Figure 6 shows the pressure profile computed for a typical highly loaded case using elements of degree 12. In fact this case uses the same non-dimensional loading parameters as in [24] although the results here have been computed with higher degree elements (elements of degree 8 and 10 are used in [24] however those results are not reproduced here since they are almost identical and would be indistinguishable if plotted on the same graph). A history of the h-adaptivity in the region around the pressure spike, using elements of degree 12, is shown in Fig 7. These calculations were made using values of 0.0001 and 0.00005 for Tol_1 and Tol_2 respectively.
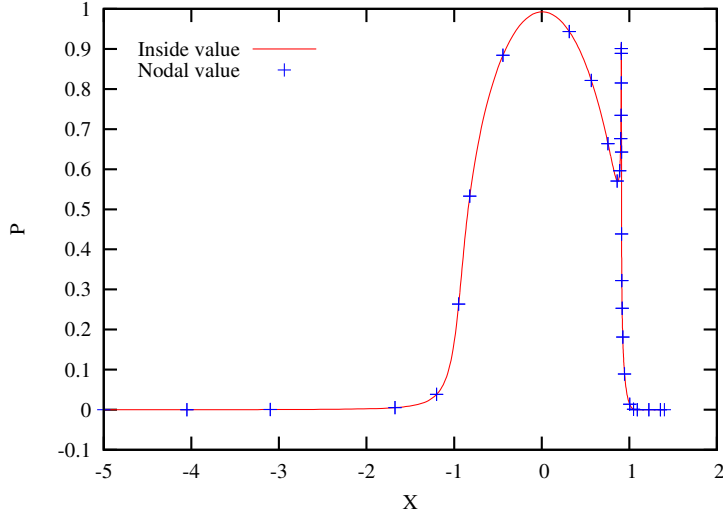
Figure 6: The pressure profile obtained for a typical line contact (see [24]) using polynomials of degree 12.

4 Discontinuous Galerkin for Transient Problems

4.1 Time-Dependent EHL Problems

The results presented in the previous section applied to steady-state EHL line contact problems. In many situations however transient features are important and may not be neglected. Typical examples include problems with variable loads, with reversal of the lubricant flow direction, or with non-smooth contacts (see [15] for a full discussion). In this paper we restrict attention to the latter class of transient problem, involving roughness in the contact between two moving surfaces. This is generally referred to as a micro-EHL contact problem [22, 39] and, for theoretical analysis, artificial roughness models (such as indentation or waviness) [39] are usually adopted. In some situations, real roughness has also been handled using numerical methods [22]. Numerical results show that the roughness can strongly affect the pressure distribution and the film thickness profile and that the transient solutions are often significantly different from their steady-state counterparts. It follows that transient analysis is of great importance if we are to be able to approach reliable numerical predictions of the real behaviour of lubricants.

The non-dimensional equations for the line contact have already been introduced for the transient case: equations (1) to (6). In the case of a non-smooth contact however we modify equation (3) slightly, replacing it by

$$H(X,T) = H_{00}(T) + \frac{X^2}{2} - \mathcal{R}(X,T) - \frac{1}{\pi} \int_{-\infty}^{\infty} \ln|X - X'|P(X',T)\, dX', \quad (34)$$

where $\mathcal{R}(X,T)$ describes the surface roughness as a perturbation to the parabolic profile. Here we adopt a very similar dimensionless model of roughness to that used
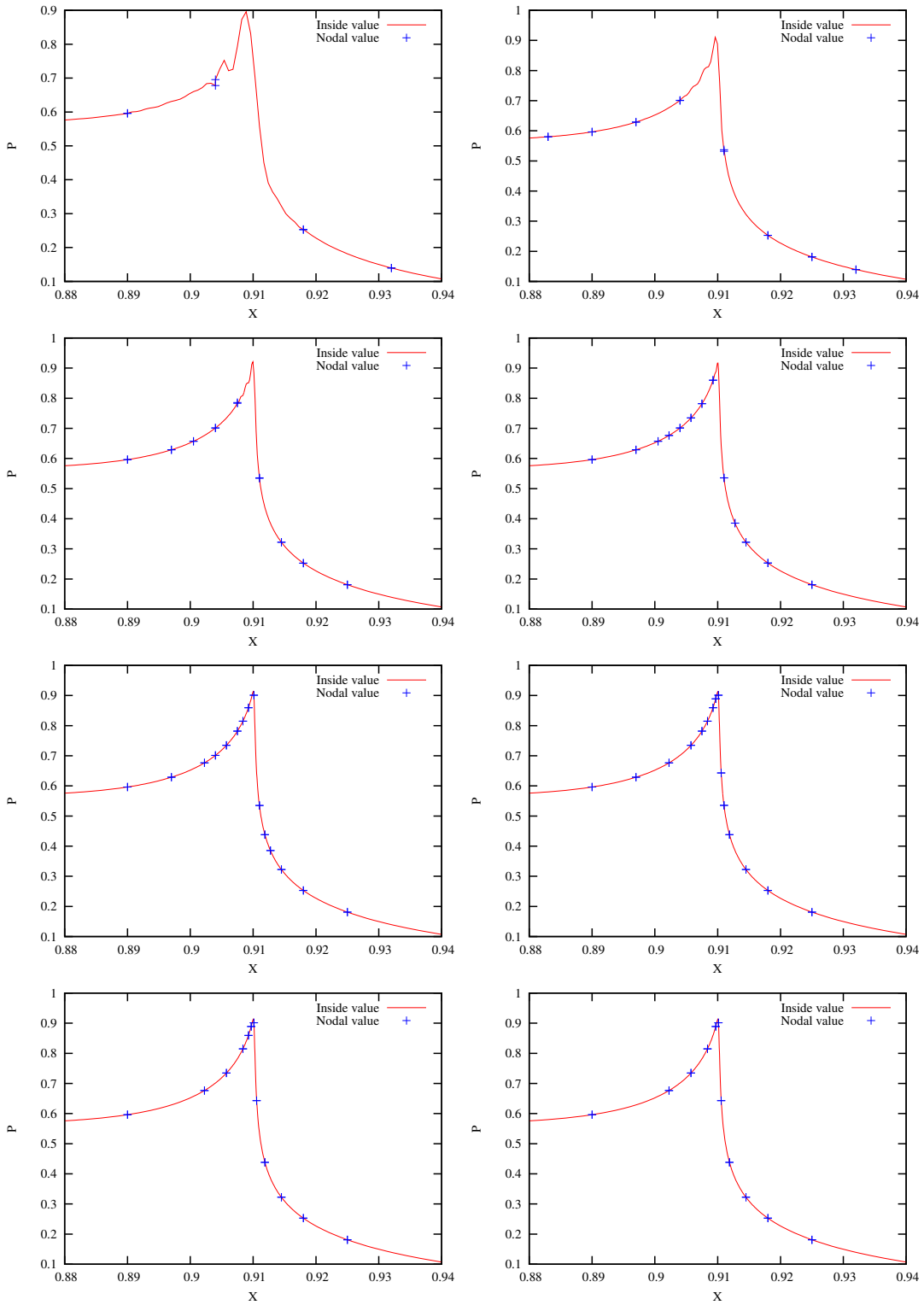
13

Figure 7: The adaptivity history in the region of the pressure spike.

14

in [39] and [25]. Specifically, we take

$$\mathcal{R}(X,T) = \alpha 10^{-40(X-X_d)^2} \cos(4\pi(X - X_d)), \qquad (35)$$

where $\alpha = -0.04$ is the amplitude of a smooth dent in the parabolic surface and X_d is the position of the centre of the dent at time T. This is given by

$$X_d = X_s + 2\frac{u_2}{u_s}T, \qquad (36)$$

where X_s denotes the position of the dent at $T = 0$, u_2 is the velocity of the indented upper surface and u_s is the sum velocity of the indented upper surface and the flat lower surface. In this example we set $\frac{u_2}{u_s} = 0.25$, hence some sliding behaviour is implied. The same loading conditions are used as in [39] and [25].

4.2   Application of the Discontinuous Galerkin Method

Recall from subsection 3.3 that the DG discretisation of the steady-state Reynolds equation using the penalty formulation leads to the nonlinear algebraic system (27) where the unknown pressure degrees of freedom in (10) are ordered as in (28). Note however that the transient form of the Reynolds equation (1) contains an additional $\frac{\partial(\rho H)}{\partial T}$ compared to the steady-state equation (7). Consequently, using the Crank-Nicolson method [22] and the DG spatial discretisation (25), the transient Reynolds equation is discretised to be:

$$-\sum_{e \in \Omega_h} \left(\int_e \rho H v \mathrm{d}x \right)^T + \sum_{e \in \Omega_h} \left(\int_e \rho H v \mathrm{d}x \right)^{T+\triangle T}$$
$$+ \theta \triangle T L(P,v)^T + (1-\theta)\triangle T L(P,v)^{T+\triangle T} = 0, \quad \forall v \in V, \quad (37)$$

where $\theta = 0.5$. The above equation allows for a single time step to be taken from T to $T + \triangle T$ and the superscripts are used to denote the time level at which the different terms are to be evaluated. Reorganising this equation, so that all of the unknown terms at time $T + \triangle T$ are grouped together, yields the following discrete form:

$$\sum_{e \in \Omega_h} \left(\int_e \rho H v \mathrm{d}x \right)^{T+\triangle T} + (1-\theta)\triangle T L(P,v)^{T+\triangle T} =$$
$$\sum_{e \in \Omega_h} \left(\int_e \rho H v \mathrm{d}x \right)^T - \theta \triangle T L(P,v)^T. \quad (38)$$

To simplify the notation further, using (10), we rewrite the above system as:

$$R^{T+\triangle T} = C(U^{T+\triangle T}) + (1-\theta)\triangle T L(U^{T+\triangle T}) - C(U^T) + \theta \triangle T L(U^T) = 0, \quad (39)$$

where L is exactly as in (27), $C(U^{T+\triangle T})$ has components $\left(\int_e \rho H N_i^e \mathrm{d}x \right)^{T+\triangle T}$, $C(U^T)$ has components $\left(\int_e \rho H N_i^e \mathrm{d}x \right)^T$ and

$$U^{T+\triangle T} = ((u_1^1)^{T+\triangle T}, \dots, (u_{p^1+1}^1)^{T+\triangle T}; \dots; (u_1^N)^{T+\triangle T}, \dots, (u_{p^N+1}^N)^{T+\triangle T}) \quad (40)$$

are the unknown pressure coefficients at the new time level. At each time step, $U^{T+\triangle T}$ must be obtained from (39) based on the known values of U^T at the previous step. It is assumed that an initial pressure profile (and therefore the values of U^T when $T = 0$) is given.

4.3 Solution Method

Similar to the nonlinear smoother introduced for the steady-state problems, the following relaxation method is used to define an iterative solver for (39) at each time step:

$$U^{T+\triangle T} \leftarrow U^{T+\triangle T} + \left(\frac{\partial \left(C(U^{T+\triangle T}) + (1 - \theta)\triangle T L(U^{T+\triangle T}) \right)}{\partial U^{T+\triangle T}} \right)^{-1} R^{T+\triangle T}, \quad (41)$$

where $R^{T+\triangle T}$ is the current numerical residual and $U^{T+\triangle T}$ is initialised to be equal to U^T. According to equation (31), the Jacobian, $\frac{\partial L(U^{T+\triangle T})}{\partial U^{T+\triangle T}}$, may be approximated by:

$$\frac{\partial L(U^{T+\triangle T})}{\partial U^{T+\triangle T}} \approx A(U^{T+\triangle T}) - \frac{\partial b(U^{T+\triangle T})}{\partial U^{T+\triangle T}}. \quad (42)$$

Furthermore $\partial b(U^{T+\triangle T})/\partial U^{T+\triangle T}$ may itself be approximated by a full matrix:

$$
\begin{aligned}
\frac{\partial b(U^{T+\triangle T})}{\partial U^{T+\triangle T}}_{I,J} &= \left[\frac{\partial b(U)_i^e}{\partial U_j^f} \right]^{T+\triangle T} \\
&= \left[\sum_{e\in\Omega_h} \left(\int_e \rho \frac{\partial H^e(X)}{\partial U_j^f} \frac{\partial v}{\partial X} \, \mathrm{d}X \right) \right]^{T+\triangle T} \\
&+ \left[\sum_{\Gamma_{int}} [v] \langle \rho(P^-) \frac{\partial H}{\partial U_j^f} + \frac{\partial \rho(P^-)}{\partial U_j^f} H \rangle \right]^{T+\triangle T} \\
&+ \left[\left(\rho \frac{\partial H}{\partial U_j^f} v \right) |_{X_{inlet}} \right]^{T+\triangle T} - \left[\left(\rho \frac{\partial H}{\partial U_j^f} v \right) |_{X_{outlet}} \right]^{T+\triangle T},
\end{aligned}
\quad (43)
$$

where the Ith row corresponds to the row generated with the test function $v = N_i^e(X)$ and the Jth column corresponds to the unknown U_j^f. Since $C(U^{T+\triangle T})$ has components $\left(\int_e \rho H N_i^e \mathrm{d}x \right)^{T+\triangle T}$, which involve the film thickness H, $\partial C(U^{T+\triangle T})/\partial U^{T+\triangle T}$ can also be approximated using a full matrix:

$$
\begin{aligned}
\frac{\partial C(U^{T+\triangle T})}{\partial U^{T+\triangle T}}_{I,J} &= \left[\frac{\partial C(U)_i^e}{\partial U_j^f} \right]^{T+\triangle T} \\
&= \left[\sum_{e\in\Omega_h} \left(\int_e (\rho \frac{\partial H^e(X)}{\partial U_j^f} v + \frac{\partial \rho}{\partial U_j^f} Hv) \, \mathrm{d}x \right) \right]^{T+\triangle T}.
\end{aligned}
\quad (44)
$$

A simple h-adaptivity algorithm was introduced in section 3, based upon the contributions of the highest order hierarchical basis functions on each element. The same adaptive procedure may be applied for the transient problem provided a small number of additional features are implemented. The initial mesh for each time step should be taken to be the final mesh for the previous time step and the adaptivity should be based upon the local smoothness of the solution $U^{T+\triangle T}$ computed via the update (41). When mesh adaptivity takes place it is important that both U^T and $U^{T+\triangle T}$ are transfered to the new mesh (using interpolation for local refinement and some form of restriction for local coarsening) before continuing with the existing time step. The overall solution procedure is therefore as follows.

1. At the start, the dent is located far from the contact region. The steady-state solution at $T = 0$ is calculated. Then for each time step, repeat 2-5 below.

2. Choose $u^{T+\triangle T} = u^T$ as initial guess.

3. Update $u^{T+\triangle T}$ by using (41) repeatedly (typically with an under-relaxation parameter included) until convergence to an intermediate tolerance.

4. Check if the grid needs to be updated. If yes, go to step 3 after generating the new grid according to the h-adaptivity method discussed above and transferring both $u^{T+\triangle T}$ and u^T onto the new grid.

5. Update $u^{T+\triangle T}$ by using (41) repeatedly (with the same under-relaxation parameter included) until convergence to a final tolerance.

Note that it is necessary to check the degree of smoothness for both $u^{T+\triangle T}$ and u^T on the local trial element when determining whether to coarsen the local mesh. The local mesh is coarsened only if both of the local solutions at T and $T + \triangle T$ are sufficiently smooth.

4.4 Computational Results

As with the steady-state results, we present here computations based upon the use of polynomials of degree 12 on each element. The problem solved is that defined in subsection 4.1, and the results are presented in the form of a sequence of pressure and film-thickness profiles at different times as the dent in the upper surface passes through the contact. Figure 8 shows solutions for X_d equal to -0.95, -0.8, -0.6 and -0.55, whilst Figure 9 shows solutions for X_d equal to -0.4, -0.15, 0.15, 0.6, 0.75, 0.8, 0.85 and 0.95.

In order to see some more of the detail of the micro-EHL contact, that the high order DG scheme is able to capture using less than forty elements, Figure 10 provides some close-ups of the pressure profile for selected values of X_d (equal to -0.55, 0.75, 0.8 and 0.85). In [25] it is shown that a finite difference scheme, using a similar number of degrees of freedom, is unable to capture this level of detail in the solution.
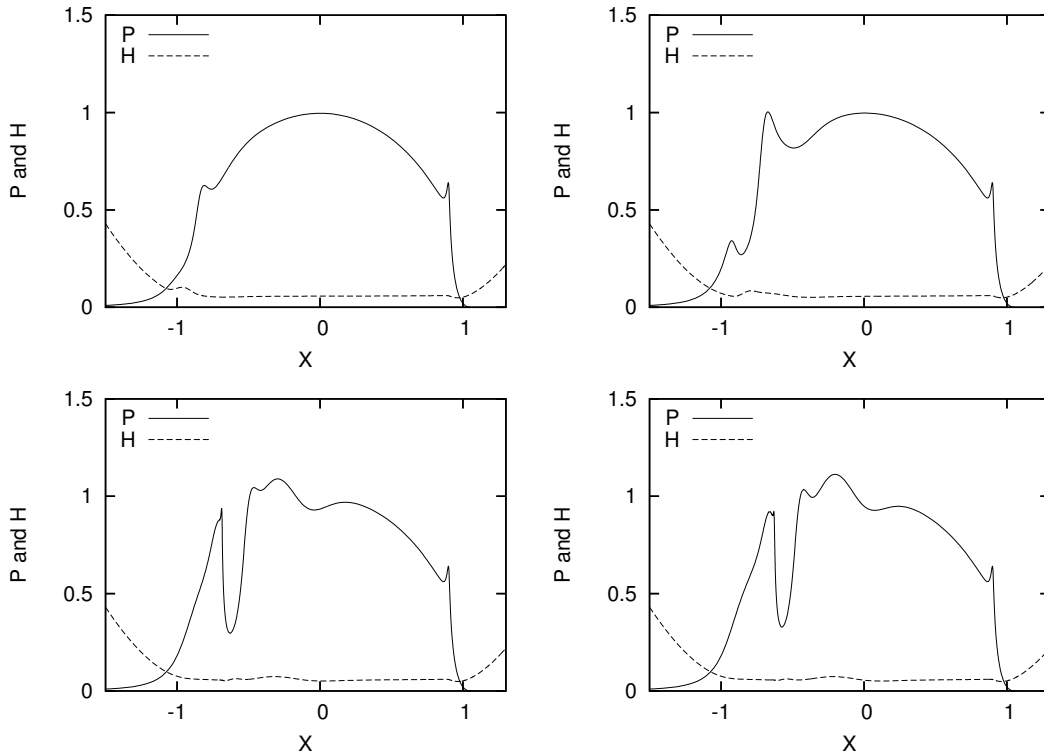
Figure 8: Computed solutions to the transient problem for X_d equal to -0.95, -0.8, -0.6 and -0.55.

5 Discussion

This paper has provided an introduction to the use of the discontinuous Galerkin method for the solution of both steady-state and time-dependent elastohydrodynamic lubrication problems. The method is ideally suited for discretising the Reynolds equation which is convection-dominated in some parts of the solution domain and diffusion-dominated in others. Results presented demonstrate that typical EHL pressure profiles, incorporating a sharp spike at the outflow of the contact and detailed micro-EHL features, may be obtained in one space dimension using only hundreds of degrees of freedom provided that a suitable adaptive strategy is used. The extension to point contacts in two space dimensions is straightforward but requires more computational work and a more complicated mesh adaptivity procedure.

Further research work is required in order to optimise the efficiency of the DG algorithm for this class of problem. In particular, the film-thickness calculation (20)-(21), requires significant memory to store all of the kernal values (especially in 2-d) and does not make use of multilevel techniques (such as MLMI, [2]) for maximum efficiency. Further improvements to the nonlinear solver for the discrete Reynolds equation are also possible and early experiments with p-multigrid methods are very promising. Overall, the DG approach appears to offer significant potential.
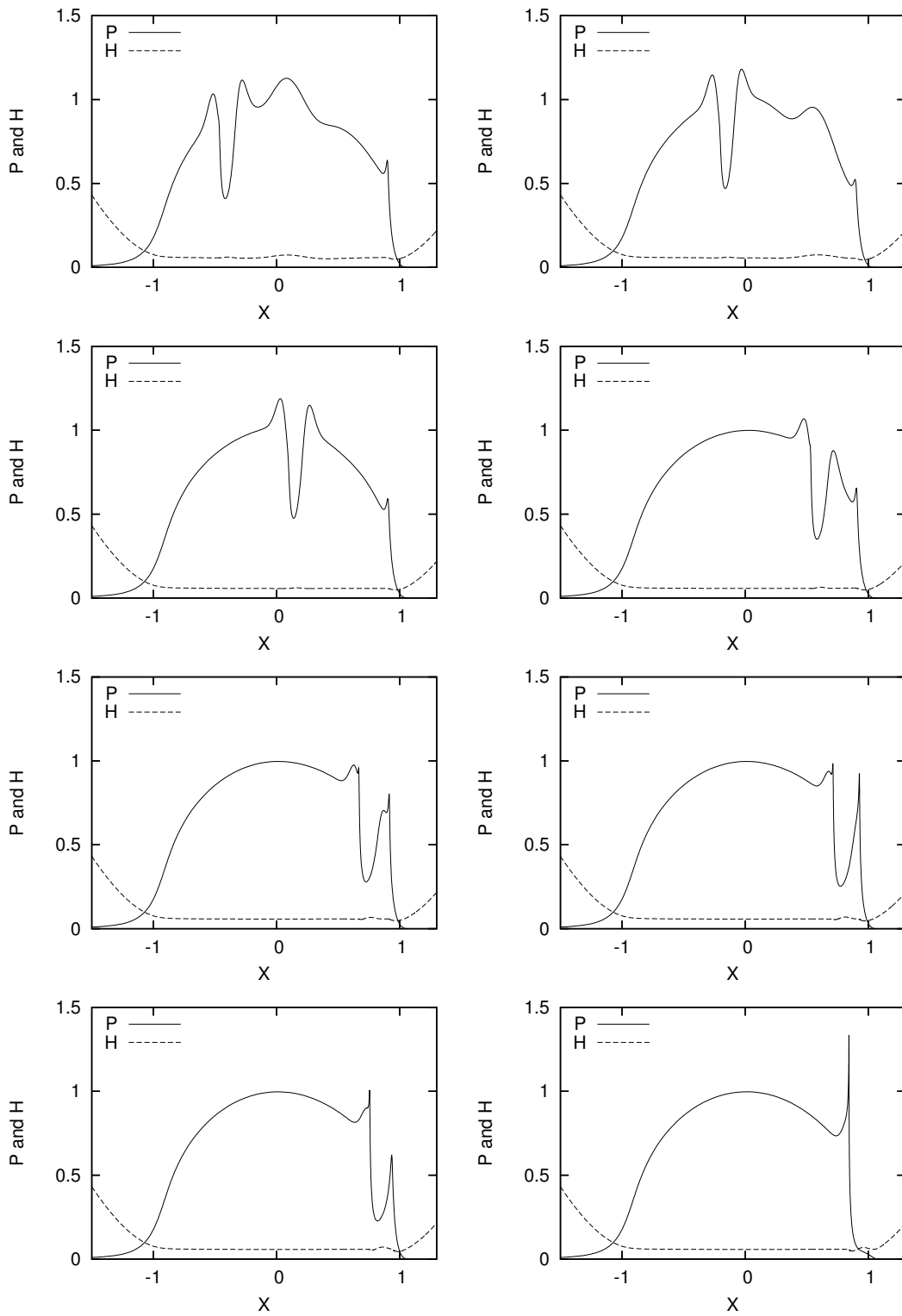
Figure 9: Computed solutions to the transient problem for X_d equal to -0.4, -0.15, 0.15, 0.6, 0.75, 0.8, 0.85 and 0.95.
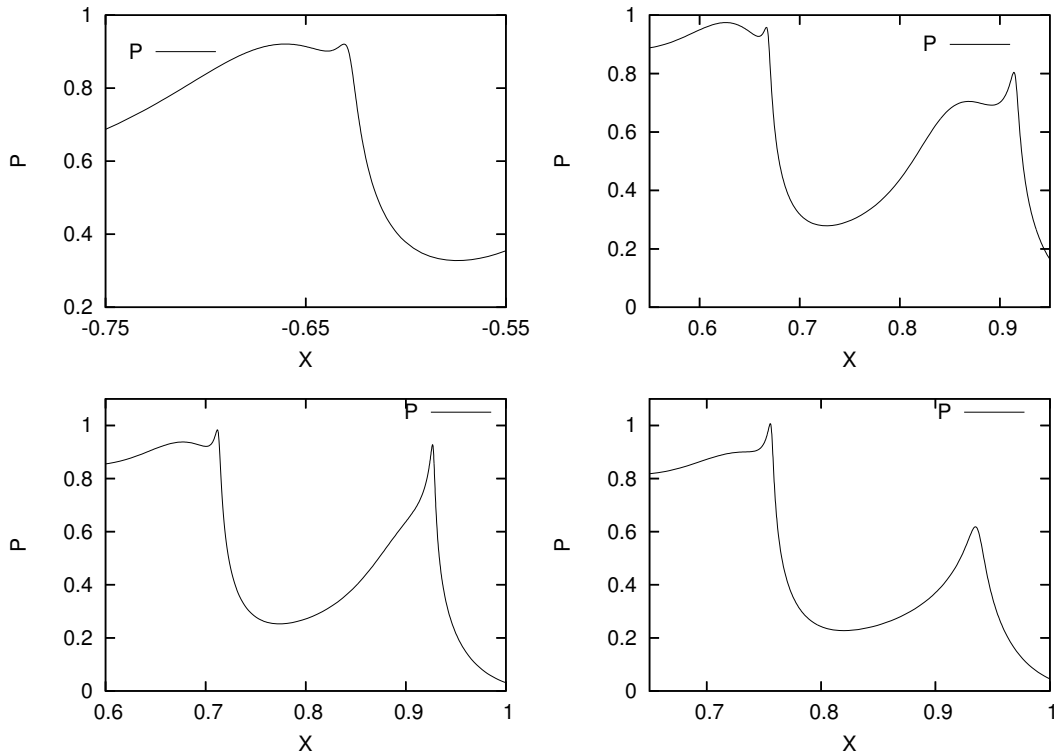
Figure 10: Computed solutions to the transient problem for X_d equal to -0.55, 0.75, 0.8 and 0.85.

References

[1] C.E. Baumann and J.T. Oden. A discontinuous hp finite element method for convection-diffusion problems. *Comput. Meth. Appl. Mech. Engrg.*, 175:311–341, 1999.

[2] A. Brandt and A.A. Lubrecht. Multilevel matrix multiplication and fast solution of integral equations. *J. Comput. Phys*, 90:348–370, 1990.

[3] B. Cockburn and Shu. C.W. TVB Runge-Kutta local projection discontinuous Galerkin finite element method for scalar conservation laws 2: General framework. *Math. Comp.*, 52:411–435, 1989.

[4] B. Cockburn and Shu. C.W. The Runge-Kutta local projection p^1-discontinuous Galerkin method for scalar conservation laws. *RAIRO Model. Math. Anal. Numer.*, 25:337–361, 1991.

[5] B. Cockburn and Shu. C.W. Runge-Kutta discontinuous Galerkin methods for convection-dominated problems. *J. Sci. Comput.*, 16:173–261, 2001.

[6] Conry T.F. Chang L. and Cusano C. An efficient robust multi-level computational algrithm for elastohydrodynamic lubrication. *ASME JOT*, 111:193–199, 1989.

[7] D. Dowson and G.R. Higginson. A numerical solution to the elasto-

hydrodynamic problem. *Journal of Mechanical Engineering Science*, 1(1):6–15, 1959.

[8] D. Dowson and G.R. Higginson. *Elasto-Hydrodynamic Lubrication, The Fundamentals of Roller and Gear Lubrication*. Pergamon Press, Oxford, Great Britain, 1966.

[9] H.P. Elcoate, C.D. Evans and T.G. Hughes. On the coupling of the elastohydrodynamic problem. *Proc. Inst. Mech. Engrs., Part J: Journal of Engineering Tribology*, 212:307–318, 1998.

[10] S.M. Eohde and K.P. Oh. A unified treatment of thick and thin film elastohydrodynamic problems by using higher order element methods. *Proc. R. Soc. Lond. A.*, 343:315–331, 1975.

[11] G. Evans. *Practical Numerical Integration*. WILEY, 1993.

[12] H.P. Evans and T.G. Hughes. Evaluation of deflection in semi-infinite bodies by a differential method. *Proc. Inst. Mech. Engrs., Part J: Journal of Engineering Tribology*, 214:563–584, 2000.

[13] H.P. Evans and R.W. Snidle. Inverse solution of Reynolds' equation of lubrication under point-contact elastohydrodynamic conditions. *ASME JOT*, 103:539–546, 1981.

[14] H.P. Evans and R.W. Snidle. The elastohydrodynamic lubrication of point contact at heavy loads. *Proc. R. Soc. Lond. A*, 382:183–199, 1982.

[15] C.E. Goodyer. *Adaptive Numerical Methods for Elastohydrodynamic Lubrication*. PhD thesis, University of Leeds, Leeds UK, 2001.

[16] B.J. Hamrock and D. Dowson. Isothermal elastohydrodynamic lubrication of point contacts, Part 1-theoretical formulation. *ASME JOT*, 98:223–229, 1976.

[17] B.J. Hamrock and B.O. Jacobson. Elastohydrodynamic lubrication of line contacts. *ASLE Transactions*, 27:275–287, 1984.

[18] Hamrock B J Hsiao HS S and Tripp J H. Finite element system approach to ehl of elliptical contacts: Part 1 - isothermal circular non-newtonian formulation. *Trans. ASME, Journal of Tribology*, 120:695–704, 1998.

[19] Hamrock B J Hsiao HS S and Tripp J H. Finite element system approach to ehl of elliptical contacts: Part 2 - isothermal results and performance formulas. *Trans. ASME, Journal of Tribology*, 121:711–720, 1999.

[20] L. Houpert and B.J. Hamrock. A fast approach for calculating film thickness and pressure in elastohydrodynamically lubricated contacts at high loads. *ASME JOT*, 108:411–420, 1986.

[21] C.D. Hughes, T.G. Elcoate and H.P. Evans. A novel method for integrating first and second order differential equations in elastohydrodynamic lubrication for the solution of smooth isothermal, line contact problems. *Int. J. Numer. Meth. Engrg.*, 44:1099–1113, 1999.

[22] Hughes T.G. Elcoate C.D., Evans H.P. and Snidle R.W. Transient elastohydrodynamic analysis of rough surfaces using a novel coupled differential deflection method. *Proc. Inst. Mech. Engrs., Part J: Journal of Engineering Tribology*, 215:319–337, 2001.

[23] C. Johnson and J. Pitkaranta. An analysis of the discontinuous Galerkin method

for a scalar hyperbolic equation. *Math. Comp.*, 46:1–26, 1986.

[24] Lu H., Berzins M., Goodyer C.E. and Jimack P.K. High order discontinuous Galerkin method for elastohydrodynamic lubrication line contact problems. *Comm. Numer. Meth. Engng.*, 21:643–650, 2005.

[25] Lu H., Berzins M., Goodyer C.E., Jimack P.K. and Walkley M.A. Adaptive high order finite element solution of transient elastohydrodynamic lubrication problems. *Proc. Inst. Mech. Engrs., Part J: Journal of Engineering Tribology*, in press, 2006.

[26] W.E. Lubrecht, A.A. ten Napel and R. Bosma. Multigrid, an alternative method for calculating film thichness and pressure profiles in ehlastohydrodynamically lubricated line contacts. *Trans. ASME, Journal of Tribology*, 108:551–556, 1986.

[27] S.H. Nguyen. A higher-order finite element scheme for incompressible lubrication calculations. *Finite Elements in Analysis and Design*, 10:307–317, 1992.

[28] I. Oden, J.T. Babuska and C.E. Baumann. A discontinuous hp finite element method for diffusion problems. *J. Comput. Phys.*, 146:495–519, 1998.

[29] K.P. Oh and S.M. Rohde. Numerical solution of the point contact problem using the finite element method. *Int. J. Numer. Meth. Engng.*, 11:1507–1518, 1977.

[30] H. Okamura. A contribution to the numerical analysis of isothermal elastohydrodynamic lubrication. *Proc. 9th Leeds-Lyon Symp. on Tribology, Leeds*, 313–320, 1982.

[31] T. Peterson. A note on the convergence of the discontinuous Galerkin method for a scalar hyperbolic equation. *SIAM J. Numer. Anal.*, 28:133–140, 1991.

[32] A.I. Petrusevich. Fundamental conclusions from the contact-hydrodynamic theory of lubrication. *Izv. Akad. Nauk. SSSR (OTN)*, 2(209), 1951.

[33] W.H. Reed and T.R. Hill. Triangular mesh methods for the neutron transport equation. *Technical Report LA-UR-73-479, Los Alamos Scientific Laboratory*, 1973.

[34] C.J.A. Roelands. *Correlational Aspects of the Viscosity-Temperature-Pressure Relationship of Lubricanting Oils*. PhD thesis, Technische Hogeschool Delft, V.R.B., Groningen, The Netherlands, 1966.

[35] T. Strouboulis and J.T. Oden. A posteriori error estimation of finite element approximations in fluid mechanics. *Comp. Meth. Appl. Mech. Engrg.*, 78:201–242, 1990.

[36] B. Szabo and I. Babuska. *Finite Element Analysis*. Wiley, New York, 1991.

[37] Taylor C. and J.F. O'Callaghan. A numerical solution of the elastohydrodynamic lubrication problem using finite elements. *J. Mech. Sci.*, 14:21–28, 1972.

[38] C.H. Venner. *Multilevel Solution of the EHL Line and Point Contact Problems*. PhD thesis, University of Twente, Endschende, The Netherlands, 1991.

[39] C.H. Venner and A.A. Lubrecht. Transient analysis of surface features in an ehl line contact in the case of sliding. *Trans. ASME, Journal of Tribology*, 116:186–193, 1994.

[40] S.R. Wu. A penalty formulation and numerical approximation of the Reynolds-Hertz problem of elastohydrodynamic lubrication. *Int. J. Eng. Sci.*, 24:1001–1013, 1986.